nature genetics

LETTERS

https://doi.org/10.1038/s41588-019-0389-8

Evolution of buffering in a genetic circuit controlling plant stem cell proliferation

Daniel Rodriguez-Leal[1,7,9], Cao Xu[1,8,9], Choon-Tak Kwon[1], Cara Soyars[2], Edgar Demesa-Arevalo[1], Jarrett Man[3], Lei Liu[1], Zachary H. Lemmon[1,7], Daniel S. Jones[2], Joyce Van Eck[4,5], David P. Jackson[1*], Madelaine E. Bartlett[3*], Zachary L. Nimchuk[2*] and Zachary B. Lippman[1,6*]

Precise control of plant stem cell proliferation is necessary for the continuous and reproducible development of plant organs[1,2]. The peptide ligand CLAVATA3 (CLV3) and its receptor protein kinase CLAVATA1 (CLV1) maintain stem cell homeostasis within a deeply conserved negative feedback circuit[1,2]. In *Arabidopsis*, *CLV1* paralogs also contribute to homeostasis, by compensating for the loss of *CLV1* through transcriptional upregulation[3]. Here, we show that compensation[4,5] operates in diverse lineages for both ligands and receptors, but while the core CLV signaling module is conserved, compensation mechanisms have diversified. Transcriptional compensation between ligand paralogs operates in tomato, facilitated by an ancient gene duplication that impacted the domestication of fruit size. In contrast, we found little evidence for transcriptional compensation between ligands in *Arabidopsis* and maize, and receptor compensation differs between tomato and *Arabidopsis*. Our findings show that compensation among ligand and receptor paralogs is critical for stem cell homeostasis, but that diverse genetic mechanisms buffer conserved developmental programs.

Plant development is driven by the replenishment of stem cells in growing apices known as meristems. In shoot meristems, the receptor kinase CLV1 and its ligand CLV3 function in a negative feedback circuit that dampens stem cell proliferation by regulating the expression of the stem cell-promoting transcription factor WUSCHEL (WUS)[1,2]. This core CLV signaling module is deeply conserved. Mutations in orthologs in the distantly related plants *Arabidopsis*, maize, rice and tomato all cause similar stem cell overproliferation, resulting in meristem enlargement and excess organs[1,2]. Mutations that partially disrupt CLV signaling have been important in domestication, making the CLV module an attractive crop improvement target[1,6]. However, both the CLV3/embryo-surrounding region (CLE) ligands and their receptors are part of large gene families[7], suggesting that CLV signaling and the phenotypic consequences arising from its perturbation could be influenced by widespread redundancy and compensation.

In *Arabidopsis*, stem cell homeostasis is mediated both through CLV–WUS negative feedback and through genetic buffering by *CLV1* paralogs[3]. The severity of the *clv1* phenotype is buffered by the paralogous BARELY ANY MERISTEM (BAM) receptors through an 'active compensation' mechanism[3,4]. In active compensation, genes change their behavior to compensate for genetic or environmental perturbation, such as the loss of a paralog. In contrast, in passive compensation, paralogs do not change their behavior under perturbation and are closer to being truly redundant[4]. Passive compensation between paralogs is often assumed, but active compensation between paralogous genes is widespread in yeast[8,9]. In the case of the *Arabidopsis* BAMs, their expression levels increase and their expression domains change when *CLV1* is compromised, compensating actively for *CLV1* loss[3]. It is unclear whether there is similar active compensation between CLE ligands, or whether compensation mechanisms are as conserved as the core CLV module[4,7].

Our previous work suggested that there is active compensation between the tomato (denoted with '*Sl*' prefix) *CLV3* ortholog, *SlCLV3* and another *CLE*, *SlCLE9*. The stem cell–repressive activity of SlCLV3 requires arabinosylation of the mature dodecapeptide[6]. *SlCLV3* expression increases 15-fold in arabinosyltransferase enzyme mutants, consistent with loss of stem cell homeostasis due to disrupted negative feedback. Interestingly, *SlCLE9* expression also increases substantially[6]. *SlCLE9* is the closest paralog of *SlCLV3*, and thus might be functionally similar to *SlCLV3* (Fig. 1a)[7]. Therefore, *SlCLE9* represented a good candidate for an active *SlCLV3* compensator in tomato.

To dissect the relationship between *SlCLE9* and *SlCLV3*, we first phenotyped *slclv3* homozygous null mutants generated by CRISPR–Cas9 and quantified the expression of both genes in meristems. As expected, *slclv3* mutants developed enlarged meristems, fasciated stems and increased floral organ and fruit locule number (Fig. 1b)[6]. Notably, both *SlCLV3* and *SlCLE9* were upregulated more than 40-fold in *slclv3* meristems, well beyond the meristem size increase (Fig. 1c). This suggested that *SlCLE9* repressed stem cell proliferation alongside *SlCLV3*. However, *slcle9* null mutants resembled wild-type (WT) plants, with a subtle effect on locule number (Fig. 1d,e, Supplementary Fig. 1a and Supplementary Table 1). Therefore, we generated *slclv3 slcle9* double mutant plants, and they were dramatically more fasciated than *slclv3* mutants, with thicker stems, more leaves and a remarkably enlarged primary shoot meristem (Fig. 1f–h and Supplementary Table 2). Side shoots showed similar phenotypes and developed severely fasciated flowers and fruits with twice as many locules as *slclv3* mutants (Supplementary Fig. 1b–d). Notably, a third *SlCLE* homolog (*SlCLE3*) was upregulated threefold in *slclv3* mutants (Supplementary Fig. 1c). However,

[1]Cold Spring Harbor Laboratory, Cold Spring Harbor, NY, USA. [2]Department of Biology, University of North Carolina at Chapel Hill, Chapel Hill, NC, USA. [3]Biology Department, University of Massachusetts Amherst, Amherst, MA, USA. [4]Boyce Thompson Institute for Plant Science, Ithaca, NY, USA. [5]Plant Breeding and Genetics Section, School of Integrative Plant Science, Cornell University, Ithaca, NY, USA. [6]Howard Hughes Medical Institute, Cold Spring Harbor Laboratory, Cold Spring Harbor, NY, USA. [7]Present address: Inari Agriculture, Cambridge, MA, USA. [8]Present address: State Key Laboratory of Plant Genomics, Institute of Genetics and Developmental Biology, Chinese Academy of Sciences, Beijing, China. [9]These authors contributed equally: Daniel Rodriguez-Leal, Cao Xu. *e-mail: jacksond@cshl.edu; mbartlett@bio.umass.edu; zackn@email.unc.edu; lippman@cshl.edu

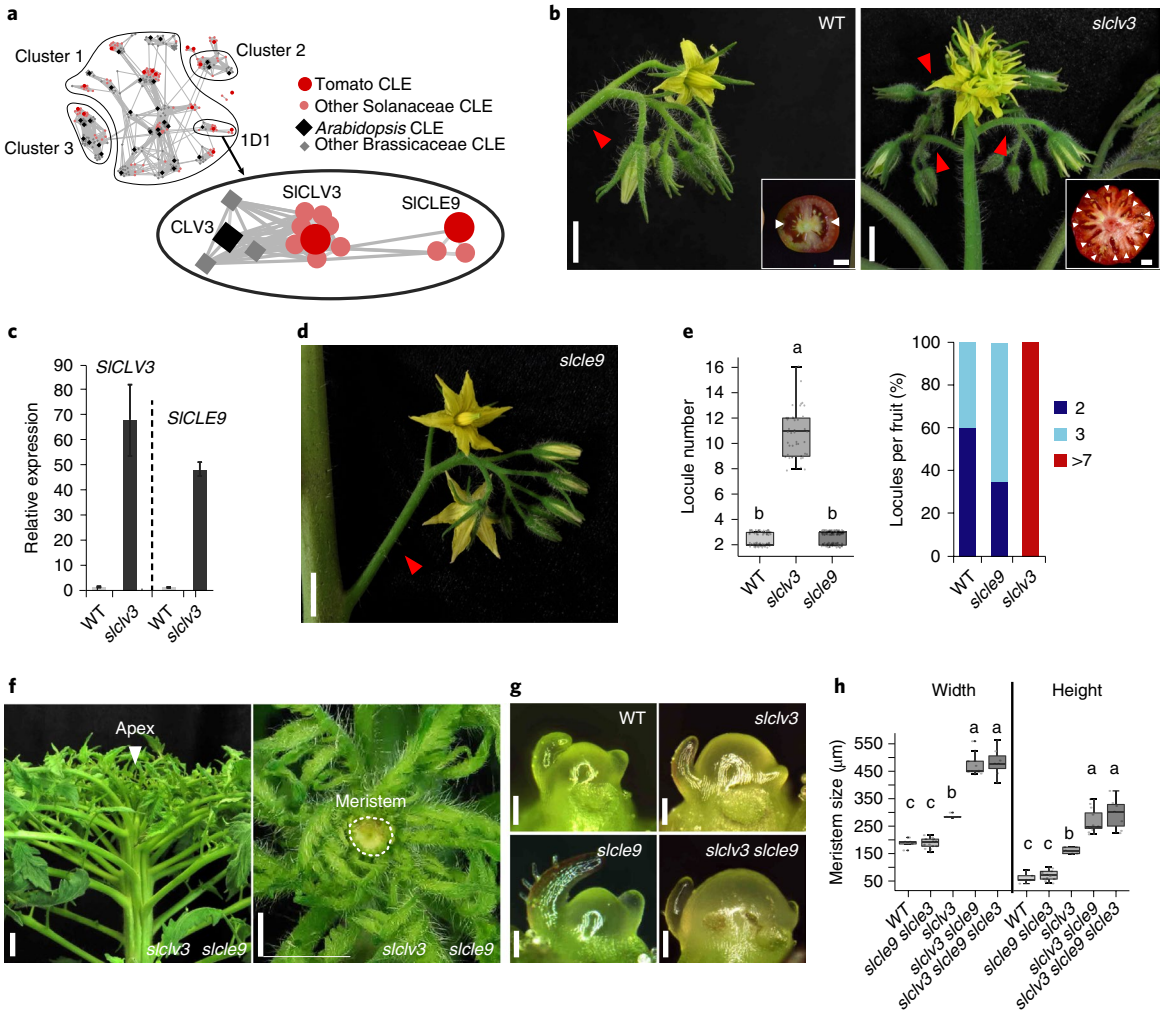

Fig. 1 | Buffering of stem cell homeostasis in tomato depends on transcriptional compensation from *SlCLE9*. **a**, Clustering of CLE proteins from Brassicaceae and Solanaceae. **b**, WT and *slclv3* tomato inflorescences. Red arrowheads, branches; white arrowheads in insets, locule number. **c**, RT–qPCR in the vegetative meristems of *SlCLV3* and *SlCLE9*, normalized to *SlUbiquitin*. Mean ± s.e.m.; two biological replicates with three technical replicates ($n = 30$ meristem per replicate). **d**, Representative inflorescence of *slcle9*. Red arrowhead, branch. **e**, Quantification and distribution of locule number in WT, *slclv3* and *slcle9* ($n = 105$, 43 and 166). **f**, Side and top-down view of *slclv3 slcle9*. White arrowhead, apex; white dotted circle, meristem. **g**, Primary meristems from WT, *slclv3*, *slcle9* and *slclv3 slcle9*. **h**, Quantification of meristem width and height from WT single and higher-order mutants ($n = 5$, 17, 5, 12 and 7). Box plots, twenty-fifth–seventy-fifth percentile; whiskers, full data range; center line, median. One-way ANOVA and Tukey test; the letters represent the significance groups at $P < 0.05$ in **e** and **h**. Scale bars: 1 cm in **b**,**d**,**f**; 100 µm in **g**.

null mutations in *SlCLE3* did not further enhance *slclv3 slcle9* double mutants or increase locule number in the *slcle9* background (Supplementary Fig. 1 and Supplementary Table 1). Thus, even though *SlCLE3* is upregulated in *slclv3* mutants, *SlCLE3* shows no evidence of compensation. In sum, loss of *SlCLV3* triggers an active compensation mechanism[4], where upregulation of *SlCLE9* buffers stem cell homeostasis in tomato.

The discovery of active *CLE* compensation in tomato prompted us to ask if similar mechanisms existed in other plants. Notably, CLV receptor and ligand mutant phenotypes in *Arabidopsis* suggested *CLE* compensation. *Arabidopsis clv1 bam1/2/3* quadruple mutants, where all CLV3 receptor function is lost, exhibit extreme meristem overproliferation, well beyond that in *clv3* mutants[3]. This phenotypic similarity to tomato *slclv3 slcle9* double mutants suggested that additional *CLE* genes could buffer stem cell homeostasis in *Arabidopsis*[3,10]. However, unlike tomato, *Arabidopsis* has no close *CLV3* paralogs (Fig. 1a). Therefore, to identify putative *CLE* compensators, we selected 18 meristem-expressed *CLE* genes (Supplementary Fig. 2a and Supplementary Table 3; see also Methods) and measured their expression in WT and *clv3* inflorescence apices (Fig. 2a). *CLV3* expression rose dramatically (>100-fold) in *clv3* mutants, as in tomato, (Fig. 2a). However, none of the other *CLE* homologs increased more than twofold. We confirmed these findings using transcriptome data, which identified no other upregulated *CLEs* (Supplementary Fig. 2b and Supplementary Table 4; see also Methods). Therefore, if any *Arabidopsis* CLEs buffer against *clv3* disruption, it is primarily through a passive compensation mechanism[4] that involves one or more *CLE* genes with little change in their expression.

To test for passive *CLE* compensation in *Arabidopsis*, we took a multiplex CRISPR–Cas9 approach. None of the existing *cle* null mutants are fasciated or have increased locule number[11,12], *CLV3* has no close paralogs and our transcriptomics yielded no clear compensator candidates (Figs. 1a and 2a, Supplementary Fig. 2b and Supplementary Table 4). This lack of clear candidates makes dissecting passive *CLE* compensation gene by gene challenging,

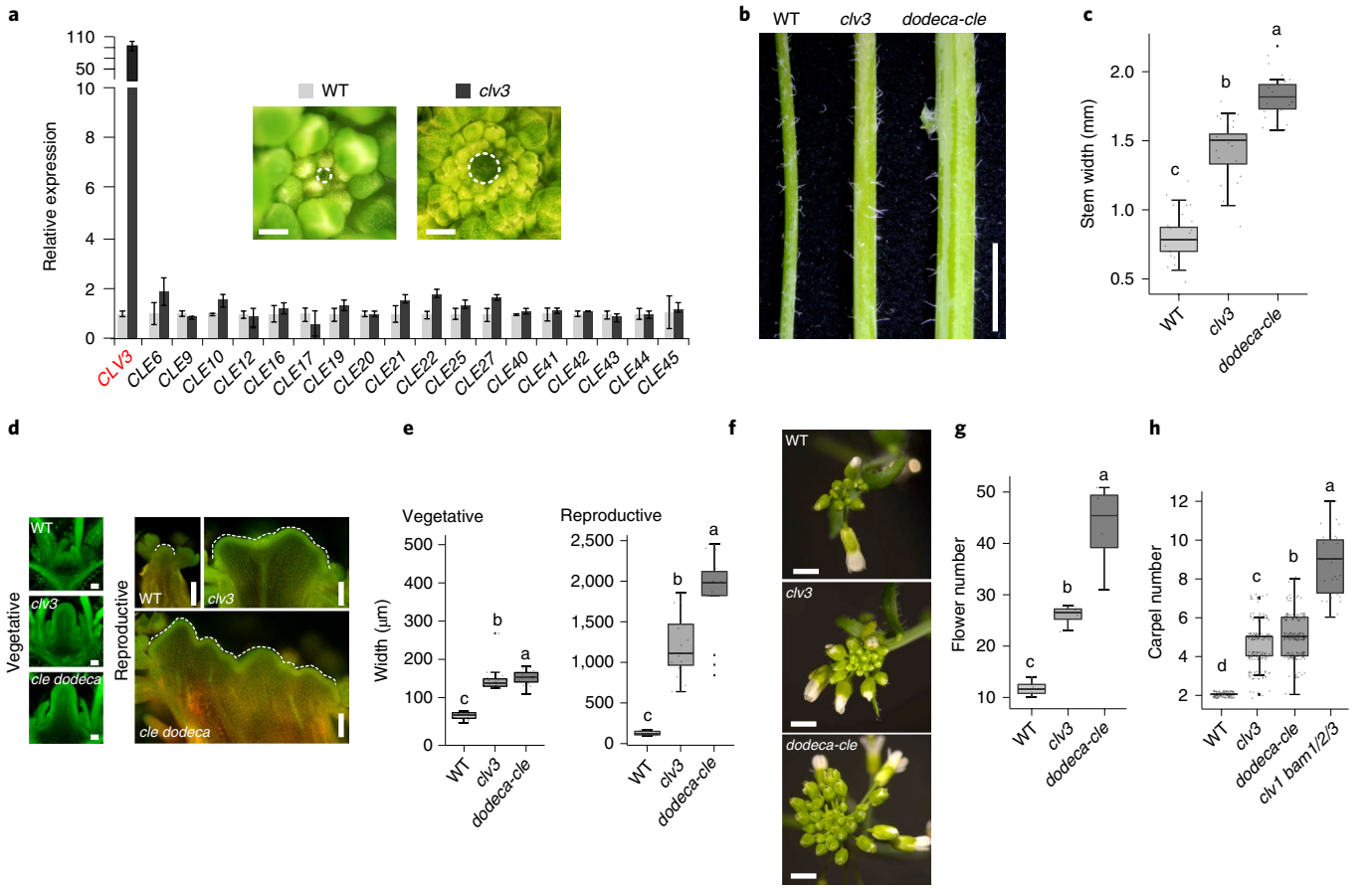

Fig. 2 | *Arabidopsis* stem cell homeostasis is controlled by multiple redundant *CLE* genes. a, RT–qPCR of *CLV3* and 18 additional *CLE* genes from inflorescence apices (dashed circles in pictures) of WT and *clv3* mutants. Normalized to *Arabidopsis thaliana UBI*. Mean ± s.e.m.; two biological replicates with three technical replicates ($n = 40$ per replicate). **b**,**c**, Representative stems (**b**) and quantification of stem width (**c**) from WT, *clv3* and *dodeca-cle* ($n = 20$, 20 and 20). **d**,**e**, Confocal micrographs of vegetative and inflorescence meristems (**d**) and meristem size quantification (**e**) from WT, *clv3* and *dodeca-cle* ($n = 26$, 30 and 29). **f**,**g**, Top-down view of inflorescences (**f**) and flower numbers (**g**) from WT, *clv3* and *dodeca-cle* ($n = 47$, 104 and 173). **h**, Quantification of locule number from WT, *clv3*, *dodeca-cle* and *clv1 bam1/2/3* ($n = 149$, 199, 199 and 26). Box plots, twenty-fifth–seventy-fifth percentile; whiskers, full data range; center line, median. One-way ANOVA and Tukey test; the letters represent the significance groups at $P < 0.05$ in **c**,**e**,**g**,**h**. Scale bars: 300 µm in **a**; 1 cm in **b**; 50 µm and 100 µm in **d;** 1 cm in **f**.

requiring many mutant combinations. This is further complicated by linked *CLE* genes. Therefore, we used multiplex CRISPR–Cas9 to simultaneously mutate 11 *Arabidopsis CLE* genes with known repressive activity in peptide assays[13], in a *clv3* mutant background. Notably, homozygous *clv3 cle* multigene mutants (hereafter referred to as *dodeca-cle*; see Methods), where nine *CLE* genes have mutations that disrupt the *CLE* dodecapeptide (Supplementary Fig. 2c), showed dramatic enhancement of stem fasciation, meristem size and flower production over *clv3* single mutants (Fig. 2b–g and Supplementary Table 2). However, this enhancement was not nearly as extreme as in *clv1 bam1/2/3* quadruple receptor mutants, and locule number was only subtly affected. This suggests that additional *CLE* genes beyond those targeted in this study buffer stem cell homeostasis (Fig. 2h, Supplementary Fig 3a,b and Supplementary Tables 1 and 2). Thus, unlike in tomato where a single *CLE* paralog compensates through active upregulation, many *CLE* genes work together to compensate passively for the loss of *CLV3* in *Arabidopsis*[4].

We next examined the relative contributions of CLV1 versus BAM receptors to compensation in both *Arabidopsis* and tomato. We found that in quadruple *clv1 bam1/2/3* receptor mutants, locule number and vegetative meristem size were both considerably increased relative to both *clv1 clv3* and *clv3 bam1/2/3* quadruple mutants (Supplementary Fig. 3). This demonstrates that in *Arabidopsis* passive *CLE* compensation is mediated by shared CLV1 and BAM receptor function. In contrast, since tomato *SlCLE9* and *SlCLV3* are close paralogs, we hypothesized that active compensation might rely on *SlCLV1* (Fig. 3a). We tested this by generating *slclv1 slclv3* double mutants, where fasciation was dramatically enhanced, approaching the severity of *slclv3 slcle9* mutants. This contrasts with *Arabidopsis*, where *clv1* does not enhance *clv3* (Fig. 3b,c, Supplementary Figs. 1d, 4b,d and Supplementary Table 1)[14]. We also generated *slclv1 slcle9* double mutants and found that *slcle9* did not enhance *slclv1* (Supplementary Fig. 4d and Supplementary Table 1). We then analyzed the transcriptome profiles from vegetative and transition meristems of WT, *slclv1* and *slclv3* single mutants, and *slclv1 slclv3* and *slclv3 slcle9* double mutants, showing that *SlCLV3*, *SlCLE9* and *SlWUS* were all upregulated to similar levels in both double mutants (Fig. 3d and Supplementary Table 5). These double mutants shared a significant overlap of differentially expressed genes (87.6% in transition meristems) compared to *slclv3* and each other (Fig. 3e). Additionally, CRISPR–Cas9-generated null mutations in *SlCLV2* (encoding the ortholog of the co-receptor CLV2) did not enhance *slclv3*, similarly to *Arabidopsis clv2 clv3* mutants (Supplementary Fig. 4)[15]. These analyses show that active *SlCLE9* compensation in tomato acts primarily through SlCLV1,

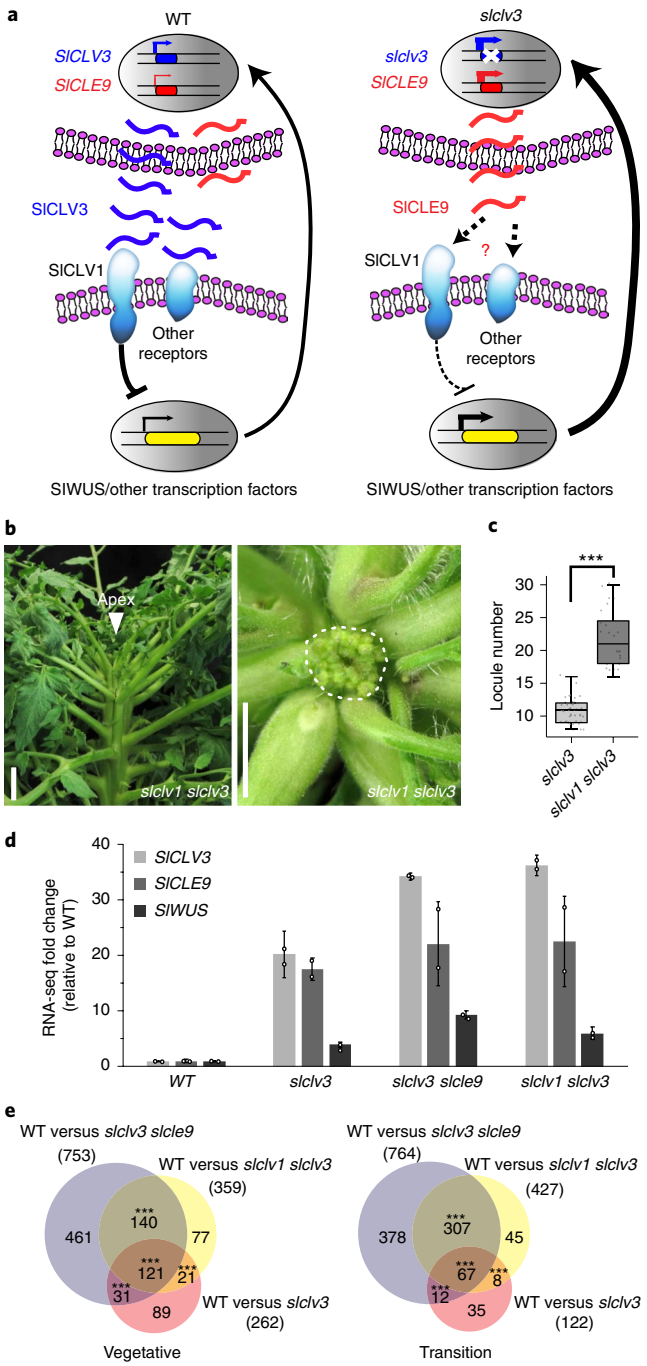

Fig. 3 | *SlCLE9* compensation acts primarily through the receptor kinase SlCLV1. a, A proposed model showing buffering of stem cell homeostasis by SlCLE9 acts primarily through SlCLV1 when SlCLV3 is compromised, achieving partial suppression of *SlWUS* through negative feedback. **b**, Side and top-down view of *slclv1 slclv3* showing an enlarged meristem flanked by multiple fasciated floral buds (dashed circle). **c**, Quantification of locule number from *slclv3* ($n = 43$) and *slclv1 slclv3* ($n = 24$). $^{***}P = 5 \times 10^{-22}$, two-tailed, two-sample *t*-test. **d**, Fold change in expression of *SlCLV3*, *SlCLE9* and *SlWUS* relative to WT RNA-seq from *slclv3* and *slclv1 slclv3*, and *slcv3 slcle9* mutants (mean ± s.d.). Data are from two biological replicates (fourfold change, 1 c.p.m. cutoff, FDR < 0.10). **e**, Venn diagrams of RNA-seq data of differentially expressed genes comparing the indicated mutant genotypes for vegetative and transition stages of meristem maturation. Box plots, twenty-fifth–seventy-fifth percentile; whiskers, full data range; center line, median. $^{***}P < 0.001$ of 1,000 simulations from random sampling. Scale bar in **b**, 2 cm.

whereas passive *CLE* compensation in *Arabidopsis* requires multiple receptor paralogs.

Since *CLE* compensation is active in tomato and passive in *Arabidopsis*, we next asked if there were similar differences in CLV receptor signaling. In *Arabidopsis*, BAM receptors are upregulated when *CLV1* is compromised in an active compensation mechanism[3]. However, transcriptome profiling in tomato showed that none of the four *BAM* (*SlBAM*) homologs[16] were dramatically upregulated in *slclv1* or *slclv3 slcle9* meristems, suggesting the lack of an active receptor compensation mechanism (Supplementary Fig. 4c). Nonetheless, we tested for active compensation genetically by disrupting the only *SlBAM* that was upregulated more than 1.5-fold in mutant meristems, *SlBAM4* (Supplementary Fig 4c). We could not distinguish *slbam4* single mutants from WT; locule number in *slclv1 slbam4* double mutants was the same as in *slclv1*. Similarly, *slbam1* single mutants and *slbam1 slbam4* double mutants had WT locule numbers, and locule number in *slclv1 slbam1 slbam4* triple mutants remained indistinguishable from *slclv1* (Supplementary Fig. 4 and Supplementary Table 1). This contrasts with *Arabidopsis*, where locule number in *clv1* mutants is enhanced stepwise by the *bam* mutants[3,17]. However, our results indicate some receptor compensation, since all available receptor mutant combinations show weaker fasciation than *slclv3 slcle9* mutants (Supplementary Fig. 4d and Supplementary Table 1). Thus, additional receptors, potentially including SlBAMs, likely contribute to SlCLV3 and SlCLE9 signaling beyond SlCLV1; however, their relative contributions appear to be different from the active compensation observed in *Arabidopsis*.

The elevated expression of *SlCLE9* in *slclv3* mutant meristems nearly matches *SlCLV3* levels in WT; however, compensation only partially masks *slclv3* stem cell homeostasis defects, suggesting that expression differences, barring possible differences in expression domains, are not responsible for the limited efficiency of *SlCLE9* compensation (Supplementary Table 5). Peptide sequence differences likely limit compensation efficiency; four amino acid substitutions distinguish SlCLE9 and SlCLV3 dodecapeptides; synthetic SlCLE9 peptides are less potent than SlCLV3 (ref. [6]). To test this genetically, we expressed the SlCLE9 dodecapeptide in the context of the *SlCLV3* gene. Whereas *slclv3* mutants were nearly fully rescued when transformed with a genomic construct containing the *SlCLV3* coding region with native upstream and downstream regulatory sequences ($gSlCLV3^{SlCLV3}$), fasciation could not be complemented by replacing the SlCLV3 dodecapeptide with that of SlCLE9 ($gSlCLV3^{SlCLE9}$) (Fig. 4a,b). Thus, active compensation efficiency is dampened by weaker activity of the SlCLE9 peptide.

The tomato domestication mutation *fasciated* (*fas*) disrupts the promoter of *SlCLV3*, reducing expression and promoting a moderate increase in locule number[6]. We hypothesized that *SlCLE9* compensation might mitigate the severity of this weaker natural *slclv3* allele. Supporting this, *SlCLE9* expression increased fourfold in *fas* meristems and still compensated, since locule number was higher in *fas slcle9* double mutants compared to *fas* alone (Fig. 4c,d). However, this enhanced fasciation did not reach the severity of *slclv3* single mutants, indicating that the *SlCLE9* compensation mechanism may scale inversely with SlCLV3 dosage. Notably, *fas* was a major contributor to increasing fruit size during domestication[6]. Our results suggest that the impact of *fas* on locule number might have been too extreme, were it not for active compensation by *SlCLE9*.

To investigate the origin of *SlCLE9* compensation, we traced the syntenic blocks containing *SlCLV3* and *SlCLE9* through eudicot evolution. Both blocks were found in the order Solanales, throughout the Solanaceae family and extending to the Convolvulaceae, as represented by *Ipomoea trifida*, the progenitor of sweet potato (Fig. 4e). Outside the Solanales, only *CLV3*-like genes were found in syntenic blocks, indicating that *SlCLE9* and *SlCLV3* originated from a Solanales-specific duplication event, although we cannot exclude the possibility of two independent duplications, specific to

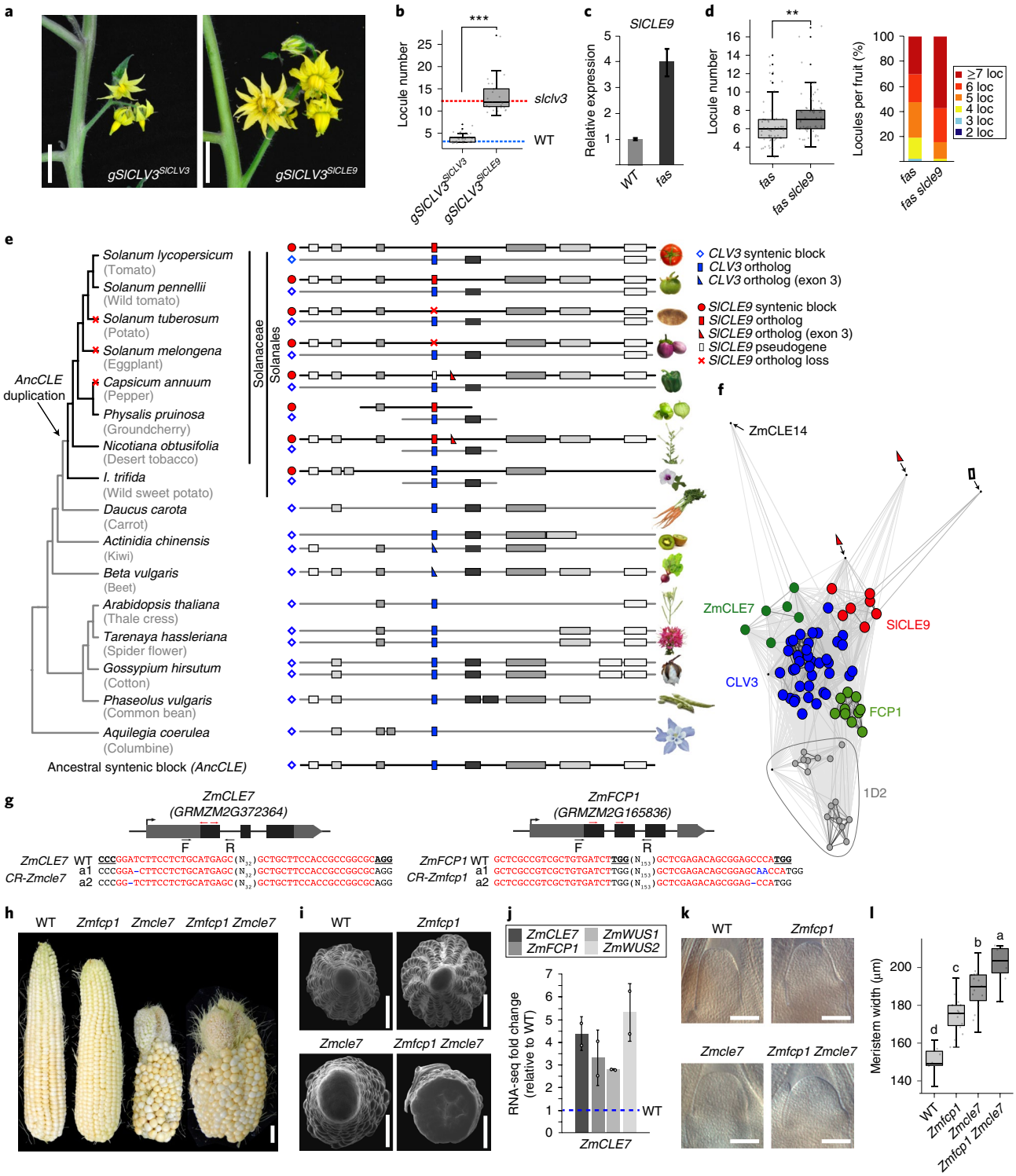

Fig. 4 | Buffering-impacted tomato domestication alongside a dynamic evolution of active compensation in flowering plants. a, Representative inflorescences from *slclv3* T_0 plants *gSlCLV3*^{SlCLV3} and *gSlCLV3*^{SlCLE9}. **b**, Quantification of locules from *gSlCLV3*^{SlCLV3} ($n=38$) and *gSlCLV3*^{SlCLE9} ($n=28$). Blue and red dashed lines, mean values for WT and *slclv3*, respectively. ***$P=1\times10^{-21}$, two-tailed, two-sample *t*-test. **c**, RT-qPCR of *SlCLE9* from the reproductive meristems of WT and *fas*. Mean ± s.e.m.; two biological and three technical replicates ($n=30$ per replicate). **d**, Quantification and distribution of locule number in *fas* ($n=59$) and *fas slcle9* ($n=59$). **$P=0.005$, two-tailed, two-sample *t*-test. **e**, Synteny analysis of the *SlCLV3* and *SlCLE9* chromosomal blocks. Red triangles, *SlCLE9*-like fragments with partial dodecapeptides. **f**, Clustering analysis of cluster 1D[7] containing *SlCLE9*-like sequences. **g**, Gene models, gRNA target sites (red arrows), primers (black arrows) and *ZmCLE7* and *ZmFCP1* CRISPR–Cas9 alleles. **h**, Representative ears and ear primordia from WT, *Zmfcp1*, *Zmcle7* and *Zmfcp1 Zmcle7*. **j**, Fold change of *ZmCLE7*, *ZmFCP1*, *ZmWUS1* and *ZmWUS2* relative to WT (dashed blue line) in RNA-seq from *Zmcle7* (mean ± s.d.; two biological replicates, twofold change, 5 c.p.m. cutoff, FDR < 0.10). **k**,**l**, Representative micrographs and quantification of inflorescence transition meristem size from WT, *Zmfcp1*, *Zmcle7* and *Zmfcp1 Zmcle7* ($n=7$, 15, 15 and 7). Box plots, twenty-fifth–seventy-fifth percentile; whiskers, full data range; center line, median. **l**, One-way ANOVA and Tukey test. Letters, significance groups at $P<0.05$. Scale bars: 1 cm in **a**,**h**; 500 μm in **i**; 100 μm in **k**.

the Solanaceae and *Ipomoea*[18,19]. Interestingly, following the emergence of *SlCLE9*, synteny within the *SlCLV3* block degraded faster than within the *SlCLE9* block[20], leaving *SlCLE9* as a clearer *CLV3* syntenic ortholog than *SlCLV3* (Fig. 4e). Once emerged, *SlCLE9*-like genes underwent a dynamic history of retention, duplication and loss, marked by two *SlCLE9*-like fragments in pepper and independent losses of *SlCLE9* from potato and eggplant (Fig. 4e and Supplementary Table 6). A broader CLE clustering supported the orthology of Solanales *CLV3*-like genes, and showed that the pepper *SlCLE9*-like sequences did not fall into any subcluster, supporting their identity as pseudogenes (Fig. 4f). Thus, *SlCLE9*-like genes likely emerged more than 30 million years ago, before Solanaceae diversification. Critically, active compensation mediated by *SlCLE9* could only have arisen after *SlCLE9* emerged, and it is specific to tomato and, potentially, its relatives in the Solanales.

Broader CLE clustering showed that the grasses, which are monocots separated from eudicots by approximately 150 million years (ref. [21]), typically harbor two closely related *CLV3*-like genes in their genomes, represented by the rice stem cell regulators *FON2* and *FCP1* (Fig. 4f)[22]. These paralogs originated from a monocot-specific duplication event, independent from the duplication leading to *SlCLV3* and *SlCLE9* (Fig. 4e,f)[7]. This mirroring between grasses and tomato led us to ask whether *CLV3*-like duplication in monocots also led to the evolution of active compensation. We mutated the maize (denoted with '*Zm*' prefix) orthologs of *FON2* (*ZmCLE7*) and *FCP1* (*ZmFCP1*) (Fig. 4g). *Zmfcp1* mutants are fasciated[23], but this phenotype was suppressed when introgressed into the standard B73 genotype (Fig. 4h,i). In contrast, *Zmcle7* null mutants had strongly fasciated ears (Fig. 4f–i). Expression profiling of *Zmcle7* inflorescence meristems showed that only *ZmCLE7* and *ZmFCP1* were significantly upregulated among 49 maize *CLEs* (Fig. 4j and Supplementary Table 7). Notably, ear fasciation was enhanced in double mutants, suggesting that *ZmFCP1* partially compensates for *Zmcle7*. However, unlike *slcle9* and *slclv3* in tomato, inflorescence transition meristems from *Zmfcp1* and *Zmcle7* single mutants were each larger in size than WT, and the effects in double mutants were additive. Thus, although maize shows the molecular hallmarks of active compensation, with another *ZmCLE* upregulated in *Zmcle7* mutants, our comparisons of the single and double mutants suggest a passive mechanism, where these *CLE* paralogs could have partially redundant roles in stem cell homeostasis (Fig. 4h–l)[23].

We have discovered the independent evolution of *CLE* compensation in monocots and eudicots, which is driven by independent gene duplication events. Given the distant relationships among *Arabidopsis*, maize and tomato, the genetic buffering of stem cell homeostasis uncovered in these species may reflect a formative feature of meristem biology. Interestingly, compensation is only partial, with compensators being less potent than the primary gene, paralleling principles of paralog compensation in yeast[8]. Partial compensators, like tomato *SlCLE9*, the *Arabidopsis* BAMs and maize *ZmFCP1* could function both to buffer stem cell homeostasis and provide developmental flexibility[24], and could participate in meristem size changes that occur during developmental transitions[25]. They could also have as-yet-undiscovered primary roles in other contexts, as is likely for the BAMs[26], maintaining subsidiary roles in shoot meristems. Similarly, paralogous gene pairs in yeast are rarely truly redundant[27,28]. While the core CLV-module is deeply conserved, our work shows that the *CLV* compensation mechanisms, which shaped at least one domestication event, are diverse. This genetic complexity of *CLV*-module compensation, which could contribute to the tolerance of CLV–WUS feedback to changes in CLV3 expression[29], identifies an underappreciated barrier to modification of these genes for crop improvement[1,30]. Our work provides a roadmap to dissect the genetic complexity underlying *CLV* compensation in other plants, and also compensation mechanisms involving other gene families in different developmental programs, which will be important for intelligent manipulation of plant development to enhance crop productivity.

Online content

Any methods, additional references, Nature Research reporting summaries, source data, statements of data availability and associated accession codes are available at https://doi.org/10.1038/s41588-019-0389-8.

Received: 18 October 2018; Accepted: 7 March 2019;
Published online: 15 April 2019

References

1. Somssich, M., Je, B. I., Simon, R. & Jackson, D. CLAVATA-WUSCHEL signaling in the shoot meristem. *Development* **143**, 3238–3248 (2016).
2. Soyars, C. L., James, S. R. & Nimchuk, Z. L. Ready, aim, shoot: stem cell regulation of the shoot apical meristem. *Curr. Opin. Plant Biol.* **29**, 163–168 (2016).
3. Nimchuk, Z. L., Zhou, Y., Tarr, P. T., Peterson, B. A. & Meyerowitz, E. M. Plant stem cell maintenance by transcriptional cross-regulation of related receptor kinases. *Development* **142**, 1043–1049 (2015).
4. Diss, G., Ascencio, D., DeLuna, A. & Landry, C. R. Molecular mechanisms of paralogous compensation and the robustness of cellular networks. *J. Exp. Zool. B Mol. Dev. Evol.* **322**, 488–499 (2014).
5. El-Brolosy, M. A. & Stainier, D. Y. R. Genetic compensation: a phenomenon in search of mechanisms. *PLoS Genet.* **13**, e1006780 (2017).
6. Xu, C. et al. A cascade of arabinosyltransferases controls shoot meristem size in tomato. *Nat. Genet.* **47**, 784–792 (2015).
7. Goad, D. M., Zhu, C. & Kellogg, E. A. Comprehensive identification and clustering of CLV3/ESR-related (CLE) genes in plants finds groups with potentially shared function. *New Phytol.* **216**, 605–616 (2017).
8. Kafri, R., Bar-Even, A. & Pilpel, Y. Transcription control reprogramming in genetic backup circuits. *Nat. Genet.* **37**, 295–299 (2005).
9. Kafri, R., Springer, M. & Pilpel, Y. Genetic redundancy: new tricks for old genes. *Cell* **136**, 389–392 (2009).
10. Nimchuk, Z. L. CLAVATA1 controls distinct signaling outputs that buffer shoot stem cell proliferation through a two-step transcriptional compensation loop. *PLoS Genet.* **13**, e1006681 (2017).
11. Yamaguchi, Y. L. et al. A collection of mutants for CLE-peptide-encoding genes in *Arabidopsis* generated by CRISPR/Cas9-mediated gene targeting. *Plant Cell Physiol.* **58**, 1848–1856 (2017).
12. Gregory, E. F., Dao, T. Q., Alexander, M. A., Miller, M. J. & Fletcher, J. C. The signaling peptide-encoding genes *CLE16*, *CLE17* and *CLE27* are dispensable for *Arabidopsis* shoot apical meristem activity. *PLoS ONE* **13**, e0202595 (2018).
13. Betsuyaku, S., Sawa, S. & Yamada, M. The function of the CLE peptides in plant development and plant-microbe interactions. *Arabidopsis Book* **9**, e0149 (2011).
14. Clark, S. E., Running, M. P. & Meyerowitz, E. M. CLAVATA3 is a specific regulator of shoot and floral meristem development affecting the same processes as CLAVATA1. *Development* **121**, 2057–2067 (1995).
15. Kayes, J. M. & Clark, S. E. CLAVATA2, a regulator of meristem and organ development in *Arabidopsis*. *Development* **125**, 3843–3851 (1998).
16. Li, H. et al. Evolution of the leucine-rich repeat receptor-like protein kinase gene family: ancestral copy number and functional divergence of *BAM1* and *BAM2* in Brassicaceae. *J. Syst. Evol.* **54**, 204–218 (2016).
17. Deyoung, B. J. & Clark, S. E. BAM receptors regulate stem cell specification and organ development through complex interactions with CLAVATA signaling. *Genetics* **180**, 895–904 (2008).
18. Bombarely, A. et al. Insight into the evolution of the Solanaceae from the parental genomes of *Petunia hybrida*. *Nat. Plants* **2**, 16074 (2016).
19. Hoshino, A. et al. Genome sequence and analysis of the Japanese morning glory *Ipomoea nil*. *Nat. Commun.* **7**, 13295 (2016).
20. Freeling, M. et al. Fractionation mutagenesis and similar consequences of mechanisms removing dispensable or less-expressed DNA in plants. *Curr. Opin. Plant Biol.* **15**, 131–139 (2012).
21. Kumar, S., Stecher, G., Suleski, M. & Hedges, S. B. TimeTree: a resource for timelines, timetrees, and divergence times. *Mol. Biol. Evol.* **34**, 1812–1819 (2017).
22. Suzaki, T., Yoshida, A. & Hirano, H.-Y. Functional diversification of CLAVATA3-related CLE proteins in meristem maintenance in rice. *Plant Cell* **20**, 2049–2058 (2008).
23. Je, B. I. et al. Signaling from maize organ primordia via FASCIATED EAR3 regulates stem cell proliferation and yield traits. *Nat. Genet.* **48**, 785–791 (2016).
24. Abley, K., Locke, J. C. W. & Leyser, H. M. O. Developmental mechanisms underlying variable, invariant and plastic phenotypes. *Ann. Bot.* **117**, 733–748 (2016).

25. Bernier, G. The control of floral evocation and morphogenesis. *Annu. Rev. Plant Physiol. Plant Mol. Biol.* **39**, 175–219 (1988).
26. Depuydt, S. et al. Suppression of *Arabidopsis* protophloem differentiation and root meristem growth by CLE45 requires the receptor-like kinase BAM3. *Proc. Natl Acad. Sci. USA* **110**, 7074–7079 (2013).
27. Kafri, R., Levy, M. & Pilpel, Y. The regulatory utilization of genetic redundancy through responsive backup circuits. *Proc. Natl Acad. Sci. USA* **103**, 11653–11658 (2006).
28. Soria, P. S., McGary, K. L. & Rokas, A. Functional divergence for every paralog. *Mol. Biol. Evol.* **31**, 984–992 (2014).
29. Müller, R., Borghi, L., Kwiatkowska, D., Laufs, P. & Simon, R. Dynamic and compensatory responses of *Arabidopsis* shoot and floral meristems to CLV3 signaling. *Plant Cell* **18**, 1188–1198 (2006).
30. Fletcher, J. C. The CLV-WUS stem cell signaling pathway: a roadmap to crop yield optimization. *Plants (Basel)* **7**, E87 (2018).

Acknowledgements

We thank C. Brooks, A. Krainer and J. Dalrymple for their technical support; P. Keen for assistance with the tomato transformation; T. Mulligan, S. Vermylen and S. Qiao from the Cold Spring Harbor Laboratory, and staff from Cornell University's Long Island Horticultural Research and Extension Center, for assistance with plant care; and H. Shinohara and Y. Matsubayashi from Nagoya University for the tomato peptide binding assays. Initial work from Z.L.N. was supported by funds from the Virginia Polytechnic Institute and State University. The research for this study was supported by: a PEW Latin American Fellowship (no. 29661) to D.R.L.; a NIGMS MIRA award from the National Institutes of Health to Z.L.N. (award no. R35GM119614-01); an Agriculture and Food Research Initiative competitive grant no. 2016-67013-24572 of the USDA National Institute of Food and Agriculture and the Next-Generation BioGreen 21 Program SSAC (grant no. PJ01322602) from the Rural Development Administration, Republic of Korea to D.J.; an Agriculture and Food Research Initiative competitive grant no. 2015-67013-22823 of the USDA National Institute of Food and Agriculture to Z.B.L.; and the National Science Foundation Plant Genome Research Program (grant no. IOS-1732253 to J.V.E. and Z.B.L., and grant no. IOS-1546837 to D.J., M.E.B., Z.L.N and Z.B.L.).

Author contributions

These authors contributed equally: C.-T.K., C.S., E.D.A. and J.M. D.R.L. performed the tomato CRISPR and *Arabidopsis* molecular and phenotypic analyses, prepared the figures and wrote the manuscript. C.X. performed the tomato CRISPR and complementation experiments, genetic and phenotypic analyses, prepared the figures and helped edit the manuscript. C.T.K. performed the tomato CRISPR experiments, and the genetic, RNA-seq and phenotypic analyses. C.S. generated the *Arabidopsis* CRISPR knockouts, performed the plant transformations and the genetic and phenotypic analyses. E.D.A. performed the maize CRISPR experiments and the genetic and phenotypic analyses. L.L. performed the maize RNA-seq analyses. J.M. performed the synteny and CLE clustering analyses. Z.H.L. performed the tomato RNA-seq analyses. D.S.J. performed the *Arabidopsis* genetic and phenotypic analyses. J.V.E. performed the tomato transformations. D.P.J. conceived and supervised the maize research and edited the manuscript. M.E.B. conceived, designed and guided the synteny and CLE clustering experiments and helped prepare the figures and write the manuscript. Z.L.N. conceived and supervised the *Arabidopsis* research and wrote and edited the manuscript. Z.B.L. conceived and led the research, supervised and performed the experiments, and wrote the manuscript.

Competing interests

The authors declare no competing interests.

Additional information

Supplementary information is available for this paper at https://doi.org/10.1038/s41588-019-0389-8.

Reprints and permissions information is available at www.nature.com/reprints.

Correspondence and requests for materials should be addressed to D.P.J., M.E.B., Z.L.N. or Z.B.L.

Methods

Plant materials and growth conditions. Seeds of tomato cultivar M82 and derived CRISPR mutants used for plant phenotyping were directly sown and germinated in soil on 96-cell plastic flats and grown as described previously[31]. *Arabidopsis* plants were grown under continuous light conditions at 25 °C. The mutant *clv1-101*, *clv3-9*, *bam1-4*, *bam2-4* and *bam3-2* alleles in the isogenic Col-0 background used in this study are from a previous report and were genotyped as described therein[4]. Double and higher-order mutants not generated using CRISPR were created by standard crossing; appropriate genotypes were selected using gene-specific mutant genotyping primers. Maize CRISPR–Cas9-derived mutants and WT segregants were sown directly on soil and grown under standard long-day greenhouse conditions (16 h light/8 h dark photoperiod) or in the field.

Plant phenotyping. Tomato meristem imaging and size measurement were performed as described previously[7,32]. Briefly, hand-dissected tomato meristems at late vegetative and transition meristem stages (11 and 13 d after germination) were captured on a Nikon SMZ1500 stereoscopic microscope. The images of *Arabidopsis* inflorescence apices were captured similarly. For quantifying meristem width in *Arabidopsis*, five-week-old inflorescence meristems from Col-0 (WT), *clv3-9* (*clv3*) and *dodeca-cle* were removed, hand-dissected and fixed in FAA (2% formaldehyde, 5% acetic acid, 60% ethanol) overnight at 4 °C. Tissue was dehydrated in an ethanol series (70, 80, 95 and 100%) for 30 min each at room temperature and cleared in methyl salicylate overnight. Meristems were mounted in methyl salicylate in a glass-bottom petri dish (catalog no. P35G-1.5-10-C; MatTek Corporation) and imaged on an inverted Zeiss LSM 710 confocal microscope. The signal corresponds to structural autofluorescence following excitation with a 488 nm Argon laser and emission detected in two broad windows (green: 504–597 nm; red: 629–731 nm). Images were edited and processed with ImageJ v.2.0.0-rc-68/1.52e (National Institutes of Health) where gamma was adjusted (0.5) to ensure complete delineation of the L1 layer of the inflorescence meristems. (Intensity data were not used for any downstream analysis.) Measurements were made in ImageJ, spanning the width of the meristem where the first primordia were visible on each side. Since *clv1 bam1/2/3* quadruple mutants rarely make a main inflorescence, vegetative meristems from seedlings were compared across genotypes. Seedling meristem perimeter, width and height in *Arabidopsis* were analyzed in 10-d-old seedlings grown on ½ Murashige and Skoog media plates lacking sucrose for Col-0 (WT), *clv3-9* (*clv3*), *clv1-101* (*clv1*), *dodeca-cle*, *clv1-101 clv3-9* (*clv1 clv3*), *bam1/2/3*, *clv-1-101 bam1/2/3* (*clv1 bam1/2/3*) and *clv3-9 bam123* (*clv3 bam1/2/3*). Plants were hand-dissected to expose the meristems, fixed in FAA and mounted as described earlier for the inflorescence meristems. The shoot apical meristems were imaged with an inverted Zeiss LSM 710 confocal microscope following the same procedure as for the inflorescence meristems. Shoot apical meristem measurements were made in ImageJ. The perimeter measurement spanned the entirety of the meristem excluding the primordia. The width was measured spanning the width of the meristem where the first primordia were visible on each side, while the height was measured spanning from the outer top portion of the meristem to the bottom portion where the meristem and primordia differentiate ($n > 10$ for each genotype imaged). For the *Arabidopsis* locule number quantifications, the primary inflorescences of independent individuals per genotype were analyzed; mature, opened flowers were counted. Specific *n* values differ (see figures for the actual numbers). For *clv1 bam1/2/3* mutant plants, the main inflorescence rarely bolts and flowers were counted from lateral shoots as necessary. To quantify *Arabidopsis* flower production, all mature flowers (fully open and with perianth organs abscised) were counted on the main inflorescence stems by eye. *Arabidopsis* stem fasciation measurements were taken with a digital Swiss Precision Instruments caliper (model no. 15-719-8) 70 mm up from the rosette of 25-day-old plants. For the quantification and imaging of maize meristems and ears, the following genotypes were obtained from a segregating F_2 population from a cross between *Zmcle7* and *Zmfcp1* CRISPR–Cas9-generated mutants: B73 (WT), *Zmcle7 Zmfcp1*/+ (*Zmcle7*), *Zmcle7*/+ *Zmfcp1* (*Zmfcp1*) and *Zmcle7 Zmfcp1*. Apices were dissected and imaged directly in the scanning electron microscope (Hitachi S-3500N) or fixed and cleared for measuring, as described for *Arabidopsis*.

CRISPR–Cas9 constructs for generating tomato, *Arabidopsis* and maize *CLE* mutants. To generate CRISPR–Cas9 mutants in tomato, a binary plasmid was built containing a functional Cas9 driven by a constitutive promoter (cauliflower mosaic virus 35S) and two guide RNAs (gRNAs) each driven by the *Arabidopsis U6* (*AtU6*) promoter using Golden Gate cloning[31,33,34]. The final binary vectors were introduced into the M82 tomato line by *Agrobacterium tumefaciens*–mediated transformation as described previously[33,35]. First-generation (T_0) transgenic plants were transplanted in soil and grown under greenhouse conditions. Genotyping of CRISPR–Cas9-generated mutations was performed as described previously[31]. Stable non-transgenic, homozygous plants were used for phenotyping and crosses. The CRISPR–Cas9 construct for producing the *Arabidopsis dodeca-cle* mutant was built using the pCUT vector system[36]. Twelve 20–base pair (bp) gRNA target sites were selected upstream of the dodecapeptide coding region in the genomic sequence of each target *CLE* gene. Three separate gRNA array genes were synthesized by GeneArt Gene Synthesis (Thermo Fisher Scientific) as groups of four *AtU6::gRNA* tandem constructs[36], which were cloned together by restriction enzyme digestion into the recipient GeneArt pMA plasmid to generate a single vector hosting 12 gRNA units. The 12-stacked gRNA unit was then cloned into the pCUT4 binary vector as described in Peterson et al.[36]. A separate set of 12 stacked gRNA units were cloned into the pCUT6 binary vector; *clv3-9* plants were transformed with the pCUT4 CRISPR binary construct by floral dipping, and the T_1 transgenic seed derived was selected on B5 media lacking sucrose and containing 100 mg l^{-1} hygromycin. T_1 plants were screened for editing efficiency by sequencing the *CLE* gene PCR products from leaf DNA. Plants were scored as having efficient editing by confirmation of overlapping sequencing traces originating at the −3 position from the protospacer-adjacent-motif site. Since no obvious phenotypes were observed in T_1 plants, and no homozygous mutants in the T_1 were expected[36], T_2 seed was sown on selective B5 media and DNA was collected from T_2 plants. Each targeted *CLE* gene was amplified with PCR, and products were directly sequenced via Sanger sequencing. We noted that some gRNAs from the pCUT4 set did not appear to work; a heterozygous pCUT4 T_2 line was transformed with the pCUT6 gRNA set to target the remaining *CLE* genes and potentially obtain larger deletion mutations. From the T_2 generation of this transformation, higher-order *CLE* mutant combinations were identified that contained lower-order homozygous fixed alleles; from those plants, the next generation was screened on hygromycin-containing B5 media, and Basta, to identify heterozygous *Cas9* transgenic plant lines. A select line was propagated to the T_3 generation and subjected to additional rounds of sequencing. Since no obvious phenotypes arose in the T_3generation, this process was continued until homozygous mutants were selected for all *CLE* genes by the T_6 generation. Plants lacking *Cas9* were confirmed by PCR and screening on both Basta and hygromycin plates. *CLE* genes from *Cas9*-free mutants were re-sequenced in independent plants to assure fixed mutations, and seed was propagated from a single fixed mutant plant. For generating CRISPR–Cas9 mutants in maize genes *ZmFCP1* and *ZmCLE7*, a binary plasmid was built containing a monocot-optimized Cas9 driven by the maize *UBI* (ubiquitin; *ZmUBI1*) promoter with two gRNAs per gene and introduced into the maize genotype Hi-II by *A. tumefaciens*–mediated tissue culture transformation[37]. Maize calli were genotyped by PCR at the target sites of both genes; those carrying mutant alleles were selected for plant regeneration. T_0 plants carrying mutant alleles were then backcrossed two or three times to B73 to segregate away the transgene.

RNA extraction and quantitative PCR with reverse transcription (RT–qPCR). RT–qPCR for both tomato and *Arabidopsis* was performed as described previously[32]. Briefly, total RNA from the vegetative meristems of tomato plants and dissected shoot apices from the inflorescences of *Arabidopsis* was extracted with the ARCTURUS PicoPure RNA Extraction Kit (Applied Biosystems) and the RNeasy Mini Kit (QIAGEN), respectively; 1 µg of total RNA was treated with DNase I (QIAGEN) and used for complementary DNA synthesis with a SuperScript III Reverse Transcriptase kit (Invitrogen). qPCR was performed using gene-specific primers (see Supplementary Table 8) in the iQ SYBR Green Supermix (Bio-Rad Laboratories) reaction system on the CFX96 Real-Time PCR Detection System (Bio-Rad), following the manufacturer's instructions.

Meristem transcriptome profiling. Total RNA from tomato vegetative and transition meristems was extracted using the ARCTURUS PicoPure RNA Extraction Kit from 20–40 meristems per replicate for each genotype, yielding 200–1,000 ng RNA. RNA sequencing (RNA-seq) libraries were prepared using the KAPA mRNA HyperPrep Kit (Roche). The quality of each RNA-seq library was tested with a 2100 Bioanalyzer (Agilent Technologies). Paired-end 75-base sequencing was performed on the Illumina HiSeq sequencing platform. Two biological replicates were used for all library constructions[7,32]. For maize RNA-seq, inflorescence meristems (approximately 0.5 mm) from a segregating population were dissected from growing ears (2–7 mm in length). Total RNA was extracted using the Direct-zol RNA Kit (Zymo Research) and sequenced on the NextSeq 500 platform (Illumina) at the Cold Spring Harbor Laboratory Genome Center. Reads for the WT tomato M82 and *slclv* mutants were trimmed by quality using Trimmomatic v.0.32 (parameters: ILLUMINACLIP:TruSeq3-PE-2.fa:2:40:15:1:FALSE LEADING:3 TRAILING:3 SLIDINGWINDOW:4:15 MINLEN:50)[38] and aligned to the reference genome sequence of tomato (SL3.00)[39] using TopHat v.2.1.1 (parameters: --b2-very-sensitive --read-mismatches 2 --read-edit-dist 2 --min-anchor 8 --splice-mismatches 0 --min-intron-length 50 --max-intron-length 50,000 --max-multihits 20)[40]. Alignments were sorted with SAMtools[41] and gene expression was quantified as unique read pairs aligned to reference-annotated gene features (International Tomato Annotation Group v.3.2) using HTSeq-count v.0.6.08 (parameters: --format = bam --order = name --stranded = no --type = exon --idattr = Parent)[42]. Maize RNA-seq data were trimmed with Trimmomatic v.0.36 (parameters: ILLUMINACLIP:TruSeq3-PE.fa:2:30:10:LEADING:3 TRAILING:3 SLIDINGWINDOW:4:20 MINLEN:50)[38] and aligned to the reference genome (B73 RefGen v.3)[43] using TopHat v.2.1.1 (parameters: --b2-sensitive --read-mismatches 2 --read-edit-dist 2 --min-anchor 8 --splice-mismatches 0 --min-intron-length 50 --max-intron-length 50,000 --max-multihits 20)[40]. Aligned reads were then sorted with SAMtools[41] and gene expression was quantified as unique read pairs aligned to reference-annotated gene features in the maize (B73 AGP v.3.22) using HTSeq-count

v.0.6.08 (parameters: --format = bam --order = name --stranded = no --type = exon --idattr = Parent)[42]. All statistical analyses of gene expression were conducted in R[44]. Significant differential expression between two meristem stages for tomato WT and mutant genotypes (middle vegetative meristem 'MVM' and transition meristem 'TM') and between maize inflorescence ear tips from *Zmcle7* mutants and WT siblings was identified with edgeR[45] using a fourfold change, average 1 count per million (c.p.m.) and false discovery rate (FDR) ≤ 0.10 cutoffs or a twofold change, average 5 c.p.m. and FDR ≤ 0.10, respectively[46].

Quantification and statistical analysis. For the tomato and locule number quantifications, at least three primary or secondary inflorescences from three or more individuals per genotype were analyzed. For the tomato and maize meristem measurements, at least 5 independent plants were analyzed per genotype, and 10–15 independent plants used for *Arabidopsis* fixation and inflorescence meristem imaging. For *Arabidopsis* seedling meristem measurements, 11–16 independent seedlings were analyzed per genotype. For the *Arabidopsis* carpel number quantifications, $n > 140$ per genotype were counted, with the exception of *clv1 bam1/2/3* mutants, which have reduced flower production owing to extreme stem overgrowth ($n = 26$). For the RT–qPCR experiments, two biological and three technical replicates were analyzed per experiment. Statistical analysis was performed using a two-tailed, two-sample Student's *t*-test and a one-way analysis of variance (ANOVA) with Tukey test ($\alpha = 0.05$). Raw data and the specific number of plants (n), meristems, flowers or fruits (n) is shown in Supplementary Tables 1 and 2. The RNA-seq differential expression analysis for tomato and maize is shown in Supplementary Tables 5 and 7. All raw data are provided in Supplementary Tables 1–8.

Transgenic complementation of *SlCLV3* and *SlCLE9*. The genomic DNA sequences of *SlCLV3* consisted of $gCLV3^{gCLV3}$ 3,261 bp in total with 1,995 bp upstream, 600 bp of coding sequence including introns and 666 bp downstream. To mutate the SlCLV3 dodecapeptide into SlCLE9 within $gCLV3^{gCLV3}$ ($gCLV3^{gSlCLE9}$), the PCR products were amplified from pDONOR221-$gCLV3^{gCLV3}$ and a vector containing the genomic region of *SlCLE9* (pDONOR221-*gCLE9*) with overlapping primers (Supplementary Table 8) by using the KOD Xtreme Hot Start DNA Polymerase (Merck Millipore). The resulting PCR products were digested with DpnI (New England Biolabs) and transformed into DH5α competent cells. Sanger sequencing confirmed pDONOR221-$gCLV3^{gCLV3}$ and $gCLV3^{gSlCLE9}$; colonies were recombined into binary vector pGWB401 (ref. [47]) for transgenic complementation.

CLE clustering. We constructed Hidden Markov Models (HMMs) particular to each CLE cluster as defined by Goad et al.[7]. We generated HMMs that included all angiosperm CLE sequences in a particular cluster, as well as Brassicaceae, Solanaceae and monocot-specific HMMs. We searched Brassicaceae, Poaceae and Solanaceae genomes with these HMMs and used the retrieved sequences ($E < 0.001$) in downstream clustering analyses. For the clustering analysis focused on CLV3 and SlCLE9, we included only those CLE propeptide sequences in cluster 1D, as well as those sequences identified in our synteny analysis (Supplementary Table 6). We submitted either all full CLE pre-propeptide sequences from Brassicaceae and Solanaceae, or only the cluster 1D CLE pre-propeptide sequences, to an all-by-all BLAST using the Bioinformatics Toolkit (Max Planck Institute for Developmental Biology)[48]; the results were visualized by clustering using CLANS v.1.0 (ref. [49]). The resulting clusters were named according to the conventions set by Goad et al.[7]. Based on the clusters formed in this analysis, the full pre-propeptide translations of *CLE* genes from clusters 1D1 and 1D2 were chosen for further analysis.

***SlCLV3* and *SlCLE9* synteny analysis.** To find genomic regions orthologous to the tomato *SlCLE9*/*SlCLV3* regions in each target species, the peptide sequences of each of the four genes flanking *SlCLE9* and *SlCLV3* were used to run CoGe BLAST v.5.6 (ref. [50]) on the target species genome using the 'tblastn' search algorithm. Groundcherry genomic fragments were obtained from Lemmon et al.[51]. For each search, the genomic regions that contained the three best matches were compared to the *SlCLE9* and *SlCLV3* regions using CoGe GEvo v.5.6 (ref. [50]) at a scale of 160,000 bp centered on the matched gene, using the 'BLastZ: Large Regions' algorithm with a score threshold of 3,000. If two or more genes in this region aligned to genes in the tomato *SlCLE9* or *SlCLV3* regions, it was considered syntenic.

CLE peptide collection from syntenic regions. For each syntenic region match, the GEvo alignment parameters were adjusted to detect CLEs, which are often missed by the default parameters. Two strategies were employed: first, the BLastZ: Large Regions algorithm with a reduced score threshold of 2,000; and second, the 'BLASTN: Small Regions' algorithm with a mismatch penalty reduced to −1. If either of these strategies found an alignment to *SlCLE9* or *SlCLV3* in the syntenic region, that portion of sequence was extracted and aligned to both *SlCLE9* and *SlCLV3* using MAFFT v.7.313 (ref. [52]), using the 'L-INS-i' algorithm and BLOSUM45 (BLOcks SUbstitution Matrix) scoring matrix. From those individual alignments, we attempted to extract a CLE peptide translation, over the full pre-propeptide, if possible, or just the dodeca region if alignment quality was poor. The *CaCLE9* pseudogene was identified by aligning the pepper genomic region syntenic to the *SlCLE9* region using MAFFT v.7.313 (ref. [52]) with a lowered gap offset value of 0.001. This aligned *SlCLE9* to an unannotated region of the pepper genome at chromosome 6 starting at position 9321808. In this alignment, the sequences that underlie the *SlCLE9* exons share approximately 80% nucleotide identity; however, the pepper sequence has stop codons in all three reading frames and a portion of what aligns to the *SlCLE9* dodecapeptide is deleted. Further analysis with eukaryotic GeneMark.hmm v.3.47 (ref. [53]) accurately predicted the three *SlCLE9* exons but predicted no exons in the orthologous pepper region. To verify genome assembly integrity at this locus, the region was amplified from pepper genomic DNA (Supplementary Table 8), and Sanger sequenced, which had no discrepancies to the assembly sequence. All efforts to find a similar feature in the potato genome failed, which suggests that the entire *CLE9* coding region is absent in potato.

Reporting Summary. Further information on research design is available in the Nature Research Reporting Summary linked to this article.

Data availability

Raw data for all quantifications are included as Supplementary Tables. All RNA-seq data from tomato are available from the National Center for Biotechnology Information. The tomato Sequence Read Archive (SRA) project and BioProject accession nos. are SRP161864 and PRJNA491365, respectively. The maize SRA projects and BioProject accessions numbers are SRR7970748, SRR7970747, SRR7970749, SRR7970750 and PRJNA494874, respectively. RNA-seq data from *Arabidopsis* was obtained from Klepikova et al.[54] and Mandel et al.[55].

References

31. Rodríguez-Leal, D., Lemmon, Z. H., Man, J., Bartlett, M. E. & Lippman, Z. B. Engineering quantitative trait variation for crop improvement by genome editing. *Cell* **171**, 470–480.e8 (2017).
32. Park, S. J., Jiang, K., Schatz, M. C. & Lippman, Z. B. Rate of meristem maturation determines inflorescence architecture in tomato. *Proc. Natl Acad. Sci. USA* **109**, 639–644 (2012).
33. Brooks, C., Nekrasov, V., Lippman, Z. B. & Van Eck, J. Efficient gene editing in tomato in the first generation using the clustered regularly interspaced short palindromic repeats/CRISPR-associated9 system. *Plant Physiol.* **166**, 1292–1297 (2014).
34. Werner, S., Engler, C., Weber, E., Gruetzner, R. & Marillonnet, S. Fast track assembly of multigene constructs using Golden Gate cloning and the MoClo system. *Bioeng. Bugs* **3**, 38–43 (2012).
35. Gupta, S. & Van Eck, J. Modification of plant regeneration medium decreases the time for recovery of *Solanum lycopersicum* cultivar M82 stable transgenic lines. *Plant Cell Tissue Organ Cult.* **127**, 417–423 (2016).
36. Peterson, B. A. et al. Genome-wide assessment of efficiency and specificity in CRISPR/Cas9 mediated multiple site targeting in *Arabidopsis*. *PLoS ONE* **11**, e0162169 (2016).
37. Char, S. N. et al. An *Agrobacterium*-delivered CRISPR/Cas9 system for high-frequency targeted mutagenesis in maize. *Plant Biotechnol. J.* **15**, 257–268 (2017).
38. Bolger, A. M., Lohse, M. & Usadel, B. Trimmomatic: a flexible trimmer for Illumina sequence data. *Bioinformatics* **30**, 2114–2120 (2014).
39. Sato, S. et al. The tomato genome sequence provides insights into fleshy fruit evolution. *Nature* **485**, 635–641 (2012).
40. Kim, D. et al. TopHat2: accurate alignment of transcriptomes in the presence of insertions, deletions and gene fusions. *Genome Biol.* **14**, R36 (2013).
41. Li, H. et al. The Sequence Alignment/Map format and SAMtools. *Bioinformatics* **25**, 2078–2079 (2009).
42. Anders, S., Pyl, P. T. & Huber, W. HTSeq: a Python framework to work with high-throughput sequencing data. *Bioinformatics* **31**, 166–169 (2015).
43. Schnable, P. S. et al. The B73 maize genome: complexity, diversity, and dynamics. *Science* **326**, 1112–1115 (2009).
44. R Core Team. R: a language and environment for statistical computing (R Foundation for Statistical Computing, 2015).
45. Robinson, M. D., McCarthy, D. J. & Smyth, G. K. edgeR: a Bioconductor package for differential expression analysis of digital gene expression data. *Bioinformatics* **26**, 139–140 (2010).
46. Lemmon, Z. H. et al. The evolution of inflorescence diversity in the nightshades and heterochrony during meristem maturation. *Genome Res.* **26**, 1676–1686 (2016).
47. Nakagawa, T. et al. Improved Gateway binary vectors: high-performance vectors for creation of fusion constructs in transgenic analysis of plants. *Biosci. Biotechnol. Biochem.* **71**, 2095–2100 (2007).
48. Zimmermann, L. et al. A completely reimplemented MPI Bioinformatics Toolkit with a new HHpred server at its core. *J. Mol. Biol.* **430**, 2237–2243 (2018).
49. Frickey, T. & Lupas, A. CLANS: a Java application for visualizing protein families based on pairwise similarity. *Bioinformatics* **20**, 3702–3704 (2004).

50. Lyons, E. et al. Finding and comparing syntenic regions among *Arabidopsis* and the outgroups papaya, poplar, and grape: CoGe with rosids. *Plant Physiol.* **148**, 1772–1781 (2008).
51. Lemmon, Z. H. et al. Rapid improvement of domestication traits in an orphan crop by genome editing. *Nat. Plants* **4**, 766–770 (2018).
52. Katoh, K. & Standley, D. M. MAFFT multiple sequence alignment software version 7: improvements in performance and usability. *Mol. Biol. Evol.* **30**, 772–780 (2013).
53. Besemer, J. & Borodovsky, M. GeneMark: web software for gene finding in prokaryotes, eukaryotes and viruses. *Nucleic Acids Res.* **33**, W451–W454 (2005).
54. Klepikova, A. V., Logacheva, M. D., Dmitriev, S. E. & Penin, A. A. RNA-seq analysis of an apical meristem time series reveals a critical point in *Arabidopsis thaliana* flower initiation. *BMC Genomics* **16**, 466 (2015).
55. Mandel, T. et al. Differential regulation of meristem size, morphology and organization by the ERECTA, CLAVATA and class III HD-ZIP pathways. *Development* **143**, 1612–1622 (2016).

Corresponding author(s): Madelaine Bartlett, Zachary Nimchuck, David Jackson, Zachary B. Lippman

Last updated by author(s): Mar 3, 2019

Reporting Summary

Nature Research wishes to improve the reproducibility of the work that we publish. This form provides structure for consistency and transparency in reporting. For further information on Nature Research policies, see Authors & Referees and the Editorial Policy Checklist.

Statistics

For all statistical analyses, confirm that the following items are present in the figure legend, table legend, main text, or Methods section.

n/a	Confirmed	
☐	☒	The exact sample size (*n*) for each experimental group/condition, given as a discrete number and unit of measurement
☐	☒	A statement on whether measurements were taken from distinct samples or whether the same sample was measured repeatedly
☐	☒	The statistical test(s) used AND whether they are one- or two-sided *Only common tests should be described solely by name; describe more complex techniques in the Methods section.*
☒	☐	A description of all covariates tested
☒	☐	A description of any assumptions or corrections, such as tests of normality and adjustment for multiple comparisons
☐	☒	A full description of the statistical parameters including central tendency (e.g. means) or other basic estimates (e.g. regression coefficient) AND variation (e.g. standard deviation) or associated estimates of uncertainty (e.g. confidence intervals)
☐	☒	For null hypothesis testing, the test statistic (e.g. *F*, *t*, *r*) with confidence intervals, effect sizes, degrees of freedom and *P* value noted *Give P values as exact values whenever suitable.*
☒	☐	For Bayesian analysis, information on the choice of priors and Markov chain Monte Carlo settings
☒	☐	For hierarchical and complex designs, identification of the appropriate level for tests and full reporting of outcomes
☒	☐	Estimates of effect sizes (e.g. Cohen's *d*, Pearson's *r*), indicating how they were calculated

Our web collection on statistics for biologists contains articles on many of the points above.

Software and code

Policy information about availability of computer code

Data collection	Data collection was performed manually and captured using microsoft Excel v16
Data analysis	Microsoft Excel v16, RStudio 1.1.383, MPI Bioinformatics Toolkit v1, CLANS ver 1.0, MAFFT ver. 7.313, L-INS-i algorithm ver7.407, BLOSUM45 scoring matrix, Noisy ver. 1.5.12, PartitionFinder ver. 1.1.1, be JTT+I, MrBayes ver. 3.2.6 ,ggtree ver. 1.12.0, CoGe BLAST, CoGe GEvo, MAFFT ver. 7.313, GeneMark.hmm version 3.47

For manuscripts utilizing custom algorithms or software that are central to the research but not yet described in published literature, software must be made available to editors/reviewers. We strongly encourage code deposition in a community repository (e.g. GitHub). See the Nature Research guidelines for submitting code & software for further information.

Data

Policy information about availability of data

All manuscripts must include a data availability statement. This statement should provide the following information, where applicable:

- Accession codes, unique identifiers, or web links for publicly available datasets
- A list of figures that have associated raw data
- A description of any restrictions on data availability

Figures 1-4, Supplementary Figures 1, 3 and 4. No restrictions on data availability. All raw data provided with submission in Supplementary Data Tables

Field-specific reporting

Please select the one below that is the best fit for your research. If you are not sure, read the appropriate sections before making your selection.

☒ Life sciences ☐ Behavioural & social sciences ☐ Ecological, evolutionary & environmental sciences

For a reference copy of the document with all sections, see nature.com/documents/nr-reporting-summary-flat.pdf

Life sciences study design

All studies must disclose on these points even when the disclosure is negative.

Sample size	Given that all genotypes analyzed were either wild type controls or stable homozygous mutants, > 3 independent biological replicates for plants and > 20 biological replicates for flowers/fruits/meristems were analyzed in each experiment for data presented in this study. For statistical analysis, two-tailed t-test and anova with tukey test at alpha < 0.05 were used.
Data exclusions	No data excluded
Replication	All presented either in Methods or Supplementary Data Tables. N = plant number and n = flower/fruit or stem number. All attempts of replication were successful and genetic status of genotypes (whether wild type or mutant) was confirmed by PCR. Raw data for phenotypic characterizations are provided in Supplementary Data Tables.
Randomization	not applicable. Each genotype was grown side by side with several replicates, and multiple times either at greenhouse or under regulated field conditions.
Blinding	not applicable. Each individual was genotyped to confirm its genetic status (wild type or mutant) before phenotypic data was collected.

Reporting for specific materials, systems and methods

We require information from authors about some types of materials, experimental systems and methods used in many studies. Here, indicate whether each material, system or method listed is relevant to your study. If you are not sure if a list item applies to your research, read the appropriate section before selecting a response.

Materials & experimental systems

n/a	Involved in the study
☒	☐ Antibodies
☒	☐ Eukaryotic cell lines
☒	☐ Palaeontology
☐	☒ Animals and other organisms
☒	☐ Human research participants
☒	☐ Clinical data

Methods

n/a	Involved in the study
☒	☐ ChIP-seq
☒	☐ Flow cytometry
☒	☐ MRI-based neuroimaging

Animals and other organisms

Policy information about studies involving animals; ARRIVE guidelines recommended for reporting animal research

Laboratory animals	No animals were used in this study.
Wild animals	No animals were used in this study.
Field-collected samples	No animals were used in this study.
Ethics oversight	not applicable

Note that full information on the approval of the study protocol must also be provided in the manuscript.